Remote Sensing of Environment 113 (2009) 1529–1539

Contents lists available at ScienceDirect

Remote Sensing of Environment

journal homepage: www.elsevier.com/locate/rse

Assessing FPAR source and parameter optimization scheme in application of a diagnostic carbon flux model

David P. Turner [a,*], William D. Ritts [a], Sonia Wharton [b], Christoph Thomas [c], Russell Monson [d,e], T. Andrew Black [f], Matthias Falk [g]

[a] Forest Ecosystems and Society, Oregon State University, Corvallis OR, USA
[b] Atmospheric Sciences, University of California, Davis CA, USA
[c] Atmospheric Sciences, Oregon State University, Corvallis OR, USA
[d] Ecology and Evolutionary Biology, University of Colorado, Boulder CO, USA
[e] Cooperative Institute for Research in Environmental Sciences, University of Colorado, Boulder, CO, USA
[f] Biometeorology and Soil Physics Group, University of British Columbia, Vancouver BC, Canada
[g] Department of Land, Air, and Water Resources, University of California Davis, Davis CA, USA

ARTICLE INFO

Article history:
Received 5 December 2008
Received in revised form 2 March 2009
Accepted 7 March 2009

Keywords:
Carbon flux
Diagnostic model
FPAR
Parameter optimization
CFLUX
Gross primary production
Ecosystem respiration
Net ecosystem exchange

ABSTRACT

The combination of satellite remote sensing and carbon cycle models provides an opportunity for regional to global scale monitoring of terrestrial gross primary production, ecosystem respiration, and net ecosystem production. FPAR (the fraction of photosynthetically active radiation absorbed by the plant canopy) is a critical input to diagnostic models, however little is known about the relative effectiveness of FPAR products from different satellite sensors nor about the sensitivity of flux estimates to different parameterization approaches. In this study, we used multiyear observations of carbon flux at four eddy covariance flux tower sites within the conifer biome to evaluate these factors. FPAR products from the MODIS and SeaWiFS sensors, and the effects of single site vs. cross-site parameter optimization were tested with the CFLUX model. The SeaWiFs FPAR product showed greater dynamic range across sites and resulted in slightly reduced flux estimation errors relative to the MODIS product when using cross-site optimization. With site-specific parameter optimization, the flux model was effective in capturing seasonal and interannual variation in the carbon fluxes at these sites. The cross-site prediction errors were lower when using parameters from a cross-site optimization compared to parameter sets from optimization at single sites. These results support the practice of multisite optimization within a biome or ecoregion for parameterization of diagnostic carbon flux models.

1. Introduction

The ability to monitor terrestrial carbon fluxes at regional to global scales is of increasing interest in relation to understanding unmanaged and managed influences of the biosphere on the global carbon cycle (Canadell et al., 2007). Satellite remote sensing potentially offers spatially continuous information on relevant land surface properties including land cover, vegetation type, vegetation structure, disturbance history, phenology, drought stress, and light use efficiency (Running et al., 1999; Turner et al., 2004). However, design of appropriate models that use this information for scaling carbon fluxes, and parameterizing these models for spatial mode application, remain significant research challenges.

In diagnostic carbon cycles models (i.e. models driven by time series data from satellites on vegetation greenness), canopy gross primary production (GPP) is generally estimated as the product of the absorbed photosynthetically active radiation (APAR) and light use efficiency (LaFont et al., 2002; Mahadevan et al., 2008). Scalars for environmental stress factors like low temperature and high vapor pressure deficit may be used to modify a base rate for light use efficiency (LUE). Autotrophic respiration is often calculated as a fixed proportion of GPP. Algorithms for heterotrophic respiration are more variable, with some using simple base rate formulations and others using multiple litter and soil carbon pools with varying turnover times.

FPAR (the fraction of incoming PAR absorbed by the canopy) is a critical input to diagnostic models and global FPAR products are now derived from multiple sensors (MODIS, Myneni et al., 2002; SeaWiFS, Gobron et al., 2006; MERIS, Gobron et al., 2008). The algorithms generally use empirical relationships or radiation transfer models. Ground validation of these FPAR products has been limited to relatively few sites at most (e.g. Turner et al., 2005; Fensholt et al., 2006) and accuracy varies widely.

* Corresponding author. Department of Forest Ecosystems and Society, Oregon State University, Corvallis OR 97331-7501, USA. Tel.: +1 541 737 5043; fax: +1 541 737 1393.
E-mail address: david.turner@oregonstate.edu (D.P. Turner).

0034-4257/$ – see front matter © 2009 Elsevier Inc. All rights reserved.
doi:10.1016/j.rse.2009.03.003

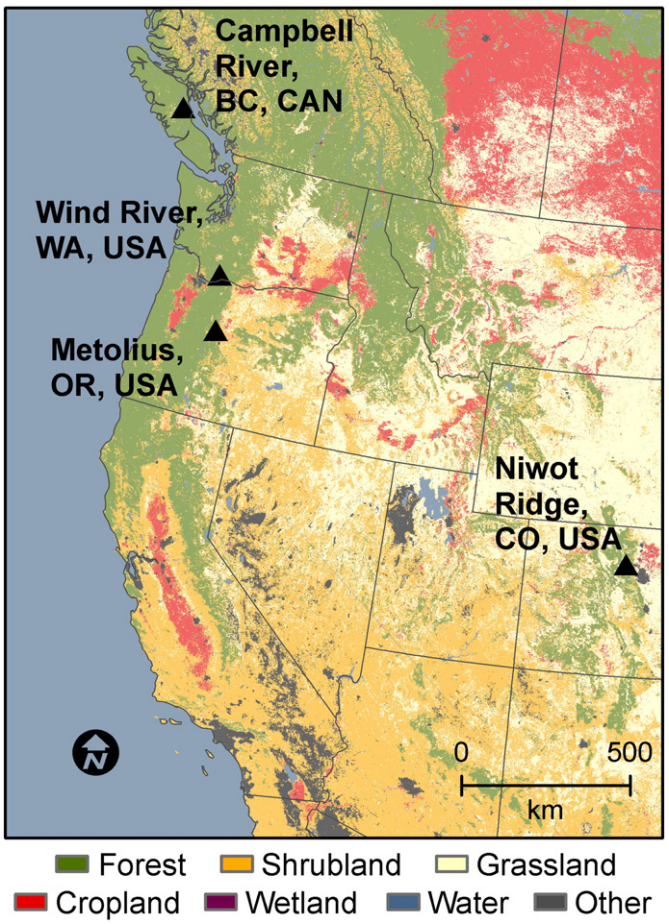

Fig. 1. Site locations. Background vegetation cover is from the MODIS sensor.

Diagnostic models tend to be kept simple enough that the parameters can be optimized from measurements. The need for parameter optimization traces in part to the limitations in satellite data, notably effects of cloudiness on FPAR. To some degree, parameter optimization compensates for possible errors elsewhere in the combination of model structure and model inputs (Medlyn et al., 2005).

In some applications, diagnostic models have been optimized across all biome types using a single set of measurements of net primary production (NPP) as reference values (e.g. Potter et al., 1993). More commonly, diagnostic models are parameterized at the biome level of vegetation stratification, the rationale being that in the case of vegetation parameters like LUE, plants make evolutionary trade-offs such that specialization for one climate regime will make it less competitive in other climate regimes. For parameters related to heterotrophic respiration (R_h), the situation is similar in that controls on decomposition rate, such as litter quality, may be characteristic of specific ecosystem types (Adair et al., 2008).

Because GPP and ecosystem respiration (R_e) can be estimated from measurements of net ecosystem exchange (NEE) at eddy covariance flux towers (Falge et al., 2002; Densai et al., 2008), establishment of a network of tower sites (Baldocchi et al., 2001) has greatly enhanced the possibilities for parameterizing and testing diagnostic models (Sims et al., 2008; Mahadevan et al., 2008). However, there has been little study of using multiple flux tower sites for parameterization within a single biome or ecoregion. Makela et al. (2008) found that responses of GPP to environmental stressors were similar across 5 conifer sites differing widely in climate but that base rates for LUE were different at each site.

In this study, we evaluate alternative FPAR sources and parameter optimization schemes for a carbon cycle diagnostic model applied at four sites in western North America dominated by conifer forests. Three years of tower data at each tower site provided the reference observations.

2. Methods

2.1. Sites

Four coniferous forest sites in western North America were used in the study (Fig. 1, Table 1). Each had a multiyear record of eddy covariance flux measurements and observations of meteorological variables. The sites varied widely in climate conditions, stand age, and leaf area index. The Campbell River site (CR) is a young Douglas-fir (*Psuedotsuga menzeisii*) stand that originated with a clear-cut harvest in 1949. The stand is located on Vancouver Island in western Canada and the climate is characterized by cool wet winters and mild dry summers. The Wind River site (WR) is an old-growth stand in the western Washington (USA) dominated by Douglas-fir and western hemlock (*Tsuga heterophylla*). Winters are colder and summers warmer than at CR. The Metolius River site (MR) is a mature ponderosa pine (*Pinus ponderosa*) stand in central Oregon (USA) that was harvested around 1920. Winters are cold and summers dry, with relatively high summer vapor pressure deficits (VPDs). The Niwot Ridge site in central Colorado (USA) was logged about 100 year ago. It is a subalpine forest dominated by Engelmann spruce (*Picea engelmanii*), subalpine fire (*Abies lasiocarpa*), and lodgepole pine (*Pinus contorta*). A late summer dry period is common at CR, WR, and MR but not at NR.

Methodology for measurement of meteorological variables and NEE at the sites are given in the references in Table 1. An index of cloudiness, for use in modifying the light use efficiency parameter (see below), was calculated as the ratio of PAR to potential PAR under clear sky conditions (Fu and Rich, 1999). Missing meteorological data were filled from nearby meteorological station data and gaps in flux observations were filled by reference to empirical functions driven by meteorological data derived from periods of good quality observations. GPP estimates were derived from observations of net ecosystem exchange (NEE) and estimates of ecosystem respiration (R_e) during daytime periods, with R_e based on relationships of nighttime NEE to air or soil temperature (Densai et al., 2008). At NR, the reference flux values were the best fit estimates from the SIPNET model fit to the NEE observations (Sacks et al., 2007). GPPs from SIPNET were of similar magnitude to GPPs modeled using the temperature/nighttime NEE approach (Sims et al., 2008).

Table 1
Site characteristics.

Site	Campbell River[a]	Wind River[b]	Metolius River[c]	Niwot Ridge[d]
Location	49°52′N, 125°20′W	45°49′N 121°57′W	44°27′N 121°33′W	40°02′N 105°33′W
Precipitation (cm)	150	247	55	80
Mean annual				
Temperature (°C)	8.5	8.7	7.5	1.5
Stand age (yrs)	56	~450	89	~100
Leaf area index (m^2 m^{-2})	8.4	8.6	2.8	4.2
fPAR (0–1)	0.95[e]	0.95[e]	0.45[f]	0.93[e]
$LUE_{clear\text{-}sky}$ (gC MJ^{-1})	1.0	1.2	0.9	0.4

$LUE_{clear\text{-}sky}$ refers to light use efficiency at the flux tower under clear skies and favorable meteorological conditions.

[a] Humphreys et al., 2006.
[b] Falk et al., 2008.
[c] Irvine et al., 2008.
[d] Sacks et al., 2007.
[e] Derived from LAI using Beer's Law (Jarvis and Leverenz, 1983).
[f] Makela et al., 2008.

2.2. Model description

A diagnostic carbon flux model (CFLUX) developed previously for application in coniferous forests was used in this study. The detailed algorithms and their rationales are given in Turner et al. (2006) and briefly described here. The model produces daily estimates of GPP, autotrophic respiration (R_a), R_h, and NEE. Daily meteorological inputs are photosynthetically active radiation, 24 h minimum temperature (Tmin), 24 h average temperature (Tavg), daytime mean vapor pressure deficit (VPD), and 24 h total precipitation. Site variables are vegetation type, stand age, and soil water holding capacity (here we used 200 mm in all cases).

The GPP estimate is based on a light use efficiency approach.

$$GPP = e_g * \downarrow PAR * FPAR \quad (1)$$

Where

GPP	Gross primary production (gC m^{-2} d^{-1})
e_g	Final LUE (gC MJ^{-1})
↓PAR	Incident photosynthetically active radiation (MJ m^{-2} d^{-1})
FPAR	Fraction of ↓PAR absorbed by the canopy.

e_g is calculated from a minimum value (based on observations at the flux tower of clear sky LUE under favorable meteorological conditions) that is adjusted upward as a function of cloudiness and downward as a function of scalars for Tmin, VPD, the soil water status, and the stand age (Turner et al., 2006).

R_a is the sum of maintenance respiration (R_m) and growth respiration (R_g).

$$R_m = R_{m\_base} * Q_{10}\text{^}((T_{air} - 20)/10) * (1/ - k)(\log(1 - FPAR)) \quad (2)$$

where

R_{m_base}	Base rate of autotrophic respiration (gC m^{-2} d^{-1})
Q_{10}	Change in rate for a 10 °C increase in temperature (here we use 2.0)
T_{air}	Daily (24 h) mean air temperature
k	Radiation extinction coefficient (here we use 0.5)
FPAR	Fraction of ↓PAR absorbed by the canopy.

The R_g component of R_a is calculated on a daily basis as:

$$R_g = (GPP - R_m) * R_{g\_frac} \quad (3)$$

Where

R_{g_frac} is the fraction of carbon available for growth that is used for growth respiration (here we used 0.25).

The R_h algorithm also uses a base rate, and contains functions for sensitivity to temperature, soil moisture, and stand age.

$$R_h = R_{h\_base} * S_{ST} * S_{SW} * S_{SA} * FPAR \quad (4)$$

Where

R_{h_base}	Base rate of heterotrophic respiration (gC m^{-2} d^{-1})
S_{ST}	Scalar for soil temperature
S_{SWh}	Scalar for soil water content
S_{SAh}	Stand age factor
FPAR	Fraction of ↓PAR absorbed by the canopy

NEE is then GPP minus R_e ($R_e = R_a + R_h$) with positive values indicating carbon uptake by the ecosystem.

CFLUX calculates a simple water balance based on precipitation as the input and evapotranspiration plus runoff as outputs. Evapotranspiration is calculated from GPP and water use efficiency.

$$ET = GPP * WUE \quad (5)$$

Where

ET	evapotranspiration (mm d^{-1})
WUE	water use efficiency (mm per gC of GPP)

A value of 0.2 mm gC^{-1} was used at all sites based on observations at a range of flux tower sites (Law et al., 2002).

2.3. FPAR data

We obtained 3 years of the standard FPAR product (collection 4.5) from the MODIS sensor for each site from the U.S.G.S. Data Archive and Analysis Center (LPDAAC, 2008). The standard FPAR product ($MODIS_{orig}$) has a spatial resolution of 1 km and is an 8-day maximum value (Myneni et al., 2002). The value is derived from a radiation transfer algorithm when possible and an empirical spectral vegetation index approach as a backup algorithm. Quality flags give an indication of which algorithm was used and the relative quality of the estimate (Cohen et al., 2006). We averaged FPAR values over a 3 cell by 3 cell window centered on the flux tower coordinates.

To minimize errors associated with low quality data, a simple linear interpolation algorithm was used to fill values for days with a low data quality flag (Zhao et al., 2005) and we applied it to the $MODIS_{orig}$ data to form a $MODIS_{fill}$ product. We also investigated the effect of a third form of FPAR in which the $MODIS_{fill}$ version is smoothed with the TIMESAT algorithm (Jonsson and Eklundh, 2004). This version ($MODIS_{TS}$) was produced by NASA for evaluation purposes (Gao et al., 2008; Nightengale et al., 2009; NACP, 2008).

We also tested an independent FPAR data set for these sites derived from the SeaWiFS sensor (Gobron et al., 2006). Spatial resolution of SeaWiFS data is ~2.2 km and temporal resolution is 10 days. As with the MODIS FPAR product, we used the Zhao et al. (2005) algorithm to fill missing data (SW_{fill}).

2.4. Parameter optimization approach

The scheme for optimizing CFLUX parameters at a single flux tower sites and year is described in Turner et al. (2006). Briefly, there are three steps. The reference data required are daily estimates for GPP and NEE, and an estimate of NPP at the site. Here we used tower-based GPP and NEE. For NPP, we assumed it was a fixed proportion of GPP based on measurements at the site (WR = 0.3, CR = 0.6, MR = 0.6) or 0.47 following Waring et al. (1998). The possible range for the parameter values is based on literature studies and preliminary model runs. The optimization may also choose to not use the temperature or VPD scalars if error is minimized by doing so. All combinations over the complete possible range of each parameter are examined.

In the first step, the five parameters controlling GPP (maximum LUE and the upper and lower bounds for the VPD and Tmin effects) are optimized using tower GPP for reference values. Minimum Root Mean Square Error (RMSE) is used as the criteria for selecting the optimum parameter set. In the second step, the optimized GPP parameters are carried over and the base rate for maintenance respiration (R_{m_base}) is optimized using the annual NPP as a reference and the minimum NPP bias as the selection criteria. Lastly, the optimized parameters for GPP and R_m are carried over and the base rate for R_h, along with parameters that determines sensitivity to temperature and the minimum FPAR (permits R_h when FPAR is artifactually low, Turner et al., 2006) are optimized using the daily-integrated NEEs as the reference values, and the minimum RMSE as the selection criteria.

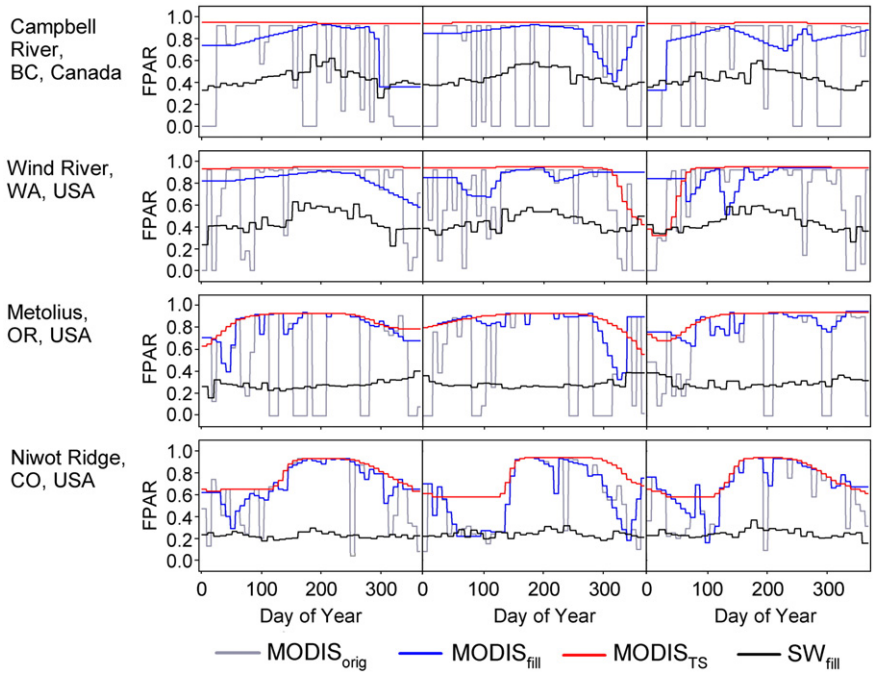

Fig. 2. Four versions of FPAR time series data. $MODIS_{orig}$ is the standard product as it comes from NASA. $MODIS_{fill}$ is the same data with missing dates filled in using the Zhao et al. (2005) algorithm. $MODIS_{TS}$ is the $MODIS_{fill}$ data smoothed with the TIMESAT algorithm (Jonsson and Eklundh, 2004). SW_{fill} is the FPAR product from the SeaWIFS sensor (Gobron et al., 2006) filled using the Zhao et al. (2005) algorithm. Years are 2002–2004 except CR (2001–2003).

To extend the optimization procedure to cover a three year interval for a site, a single RMSE was computed for the 3 years of data ($n = 1095$) in the GPP and NEE comparisons and the 3 year sum of the absolute values for the NPP bias was used in the R_{m_base} optimization. Similarly, to optimize parameters over multiple sites and years, single RMSEs and sums of absolute NPP bias were employed. All parameters except those optimized and the $LUE_{clear\text{-}sky}$ were the same in the cross-site optimization. Site level $LUE_{clear\text{-}sky}$ was retained because it was assumed that in a spatial mode application it could be retrieved from remote sensing (Drolet et al., 2008).

A cross-site, multi-year, optimization was performed for each FPAR type, then a site-level, multi-year optimization was performed for each site and FPAR type combination. For comparisons of site-level and cross-site optimizations within one FPAR type, results are presented for the case with SW_{fill} FPAR because that FPAR type yielded the lowest RMSE for NEE in the initial FPAR comparison.

3. Results

3.1. FPAR comparisons

In the $MODIS_{orig}$ FPAR product, there were multiple 8-day periods at all sites when high quality data were not available, probably because of persistent heavy cloud cover (Fig. 2). The original data from the SeaWIFS FPAR product showed a similar pattern. These periods of no data occurred during all seasons but were most prevalent in winter. The simple gap filling algorithm of Zhao et al. (2005) effectively corrected most of these problems. At CR, which does not usually experience winter snow cover, there were still some artifactual periods of low $MODIS_{fill}$ FPAR in winter. At MR (Irvine et al., 2008) and WR, there is occasional snow cover in the winter but the $MODIS_{fill}$ FPAR had no major artifacts. At NR, there is a solid snow cover all winter, which would cover some of the tree vegetation, hence the strong season signal in $MODIS_{fill}$ FPAR at NR is reasonable.

Table 2
Comparison of RMSE for gross primary production (GPP), ecosystem respiration (R_e) and net ecosystem exchange (NEE) for three forms of FPAR.

	FPAR type		
	$MODIS_{fill}$	$MODIS_{TS}$	$SeaWIFS_{fill}$
Error			
$RMSE_{GPP}$	1.68	1.55	1.67
$RMSE_{Re}$	1.54	1.43	1.45
$RMSE_{NEE}$	1.25	1.26	1.13

Parameter optimization was across all sites and all years.

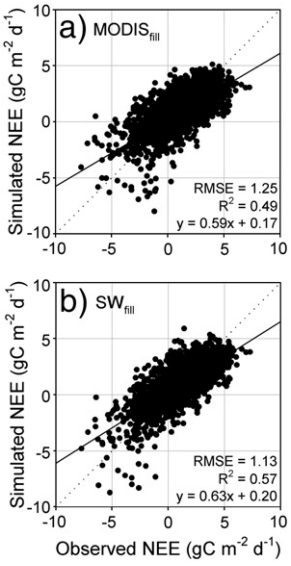

Fig. 3. Comparison of one-to-one plots of net ecosystem exchange (NEE) for the $MODIS_{fill}$ and SW_{fill} FPAR products across all sites and years. Separate parameter optimizations (one optimization across all sites + all years) were run for each FPAR product.

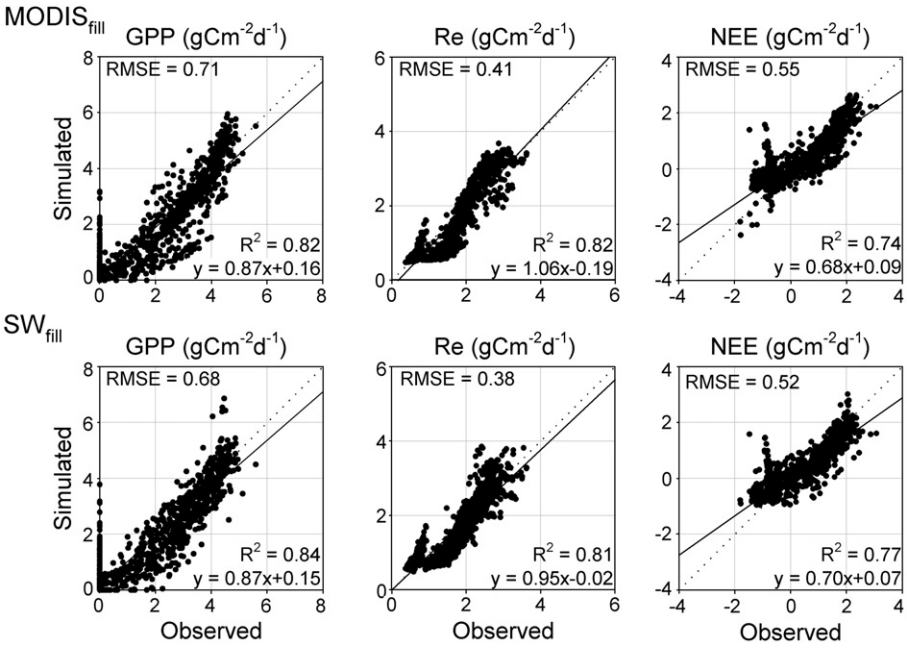

Fig. 4. Comparison of scatter plots for gross primary production (GPP), ecosystem respiration (R_e), and net ecosystem exchange (NEE) using MODIS$_{fill}$ and SW$_{fill}$ at the Niwot Ridge site. A cross site parameter optimization was used for each FPAR type.

In terms of the maximum FPAR, there was remarkably little difference in MODIS$_{fill}$ among these sites considering the great range of LAI. Summer maximum MODIS$_{fill}$ was close to 0.95 at all sites. This value is about what is predicted by a simple Beer's Law conversion of LAI to FPAR (Table 1). The Beer's Law conversion does not take into account clumping of foliage which is common in conifer stands and would tend to reduce FPAR (Stenberg, 1996). The MODIS FPARs thus appear to be overestimates at MR and NR. Interestingly, the SW$_{fill}$ FPARs exhibit more dynamic range between sites than the MODIS$_{fill}$ product but appear to be underestimates for the most part.

When parameter optimization was run across all sites and years for each FPAR type, the RMSE for GPP and the RMSE for R_e were lowest for MODIS$_{TS}$ and RMSE for NEE was lowest for SW$_{fill}$ (Table 2). In the one-to-one plot for NEE, the slope and the R^2 values were similar for MODIS$_{fill}$ and MODIS$_{TS}$ but the RMSEs were lower and the R^2 values higher for SW$_{fill}$ (Fig. 3).

The differences in FPAR resulted in different values for the optimized parameters in some cases (data not shown). The modest benefits of the greater dynamic range across sites in SW$_{fill}$ were most evident at the NR site (Fig. 4). At that subalpine site, the flux rates were generally low relative to the other sites, so in a multisite optimization its estimates for GPP and R_e tended to be high. This was much more the case with the MODIS$_{fill}$ product because there was essentially no difference in the FPARs across sites. With SW$_{fill}$, the

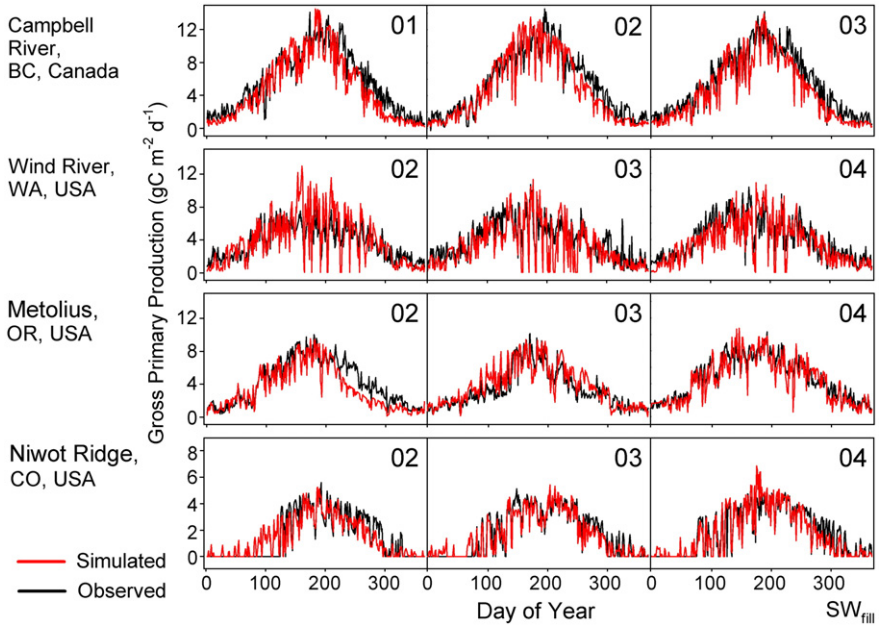

Fig. 5. Times series comparison of observed and simulated gross primary production. The SW$_{fill}$ FPAR product and site level optimizations were used. The numbers in the upper right corner of each panel refer to the year.

Table 3
Ecophysiological parameter estimates for site-specific and cross-site optimizations.

	Site				
	CR	WR	ME	NR	Cross-site
Parameter					
LUE_max (gC MJ^{-1})	4.0	3.5	4.0	3.0	4.0
Tmin_min (°C)	−12	NO[a]	−12	−8	−12
Tmin_max (°C)	4	NO[a]	6	4	4
VPD_min (Pa)	1000	0	1000	1000	0
VPD_max (Pa)	4000	2500	4000	3000	3500
R_{m_base} (gC m^{-2} d^{-1})	0.7	2.7	2.3	2.9	0.8
R_{h_base} (gC m^{-2} d^{-1})	5.0	5.8	10.0	10.0	8.8
R_{h_a} (unitless)	0.18	0.05	0.09	0.05	0.10
FPAR_min (0–1)	0.30	0.80	0.50	0.60	0.40

LUE_max is light use efficiency under conditions of maximum cloudiness. Tmin_min is the temperature at which LUE begins to be reduced. Tmin_max is the temperature at which LUE is reduced to zero. VPD_min is the vapor pressure deficit at which LUE begins to be reduced. VPD_max is the vapor pressure deficit at which LUE is reduced to zero. R_{m_base} is the base rate for maintenance respiration. R_{h_base} is the base rate for heterotrophic respiration. R_{h_a} is the temperature sensitivity coefficient for R_h. FPAR_min is the minimum value for FPAR in the R_h algorithm.
[a] NO = Not Optimized.

lower FPARs at the NR site helped bring the simulated fluxes down. As would be expected, the optimized base rates were generally lower for the MODIS FPARs compared to the SW FPARs because the MODIS FPARs were consistently higher.

3.2. Site-level optimization

3.2.1. Gross primary production

In the observations, it is clear that available ↓PAR tends to be the dominant influence on GPP in these coniferous forests. Day-to-day GPP variation is smallest at CR (Fig. 5) which also has the mildest winter and summertime temperatures. Much larger day-to-day variation in GPP is found at the other sites and appears to be driven primarily by episodes of high VPD during the main part of the growing season and low temperatures in the winter, both of which have the effect of reducing GPP. There is evidence of soil drought effects on GPP at MR (Thomas et al., in review) and WR (Falk et al., 2008) in some years.

The optimization "chose" to use the VPD scalar at all sites and it was obviously helping drive down simulated GPP on high VPD days in parallel with the observations. The optimizations also chose to use the Tmin scalar except at WR and it was obviously helping capture day-to-day variation in GPP during the winter. A significant proportion of annual GPP occurs during the winter at WR (Falk et al., 2008) which suggests little sensitivity to temperature per se. Whereas the observed clear-sky LUE varied by a factor of 3 (Table 1), optimized values for the maximum LUE ranged between 3.0 (NR) and 4.0 (MR) (Table 3).

3.2.2. Ecosystem respiration

Tower observations of R_e showed a similar seasonality to the seasonal pattern in GPP (Fig. 6). The day-to-day variability in R_e was greater at the 2 high LAI sites, probably because of the higher foliar biomass and the sensitivity of foliar respiration to air temperature. The large amount of decaying coarse woody debris at WR would also contributed to high R_h. Day-to-day variation was lowest at the coolest site (NR).

The simulations captured much of the mid-growing season day-to-day variability at CR, WR, and NR (Fig. 6). At MR, the R_h (and consequently R_e) was significantly reduced by the soil moisture scalar in each year, which appeared to match observations. The simulated reduction in R_e was too great in 2002, a year with a relatively dry spring, which suggests an overestimation of ET or underestimate of soil water holding capacity.

The optimal base rates for maintenance respiration varied by over a factor of 4 whereas the selected base rate for R_h, and the *a* parameter for R_h, varied by a factor of 2 to 4 (Table 3).

3.2.3. Net ecosystem exchange

At all sites, there is a period of positive NEE (carbon sink) in the spring and early summer followed by a sustained or fluctuating period of negative NEE (carbon source) in mid summer (Fig. 7). This pattern is most apparent at WR and least so at NR. Day-to-day variation in NEE is high at all sites. The simulations generally followed the seasonal

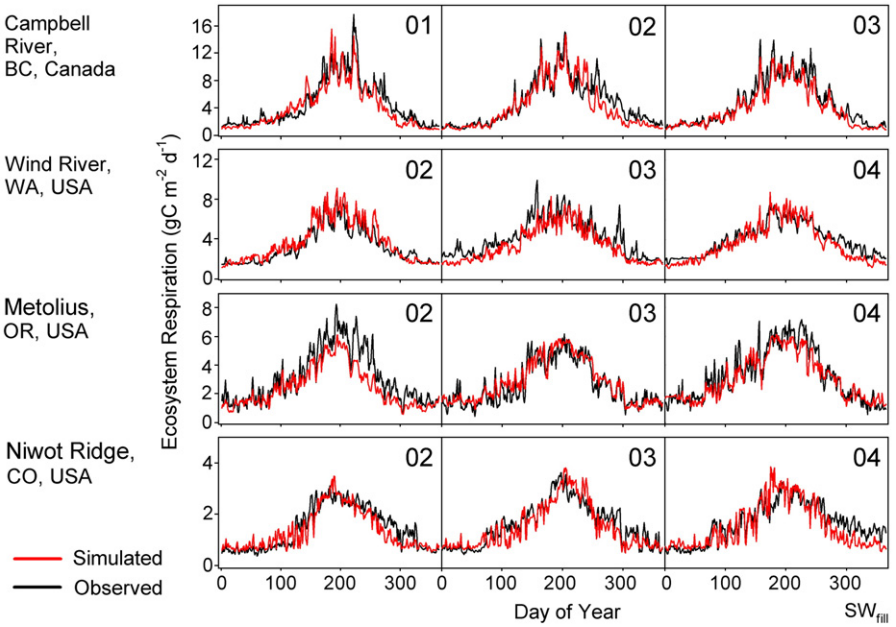

Fig. 6. Times series comparison of observed and simulated ecosystem respiration. The SW_{fill} FPAR product and site level optimizations were used. The numbers in the upper right corner of each panel refer to the year.

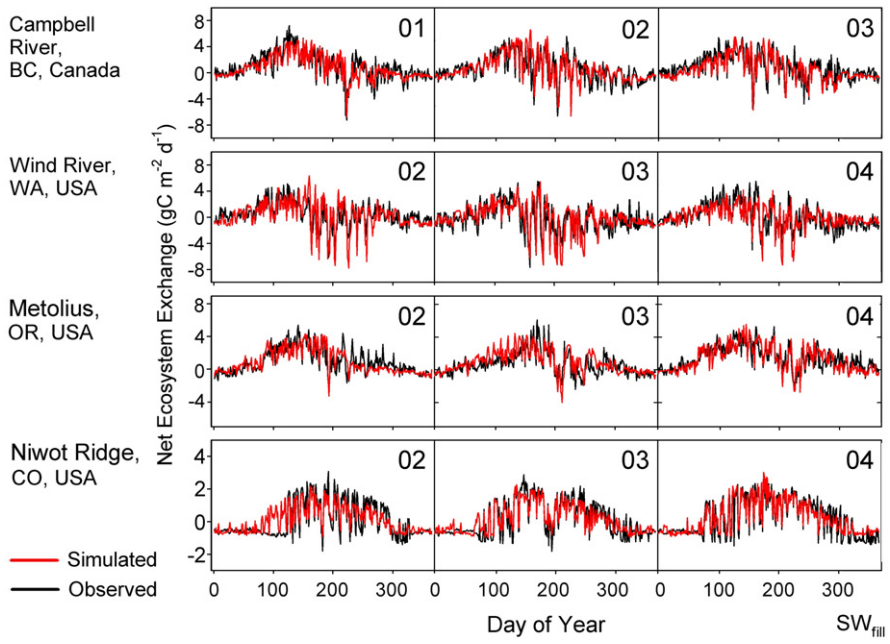

Fig. 7. Time series comparison of observed and simulated net ecosystem exchange. The SW_{fill} FPAR product and site level optimizations were used. The numbers in the upper right corner of each panel refer to the year.

trends seen in the observations and showed day-to-day variation of similar magnitude and sensitivity to environmental variation.

3.2.4. Interannual variation

NEE is usually a small difference between the much larger GPP and R_e fluxes. Thus interannual variation in either GPP or R_e tends to propagate into NEE. At the annual time step, the tower data and simulations showed a similar amount of interannual variation in GPP, R_e, and NEE. The sign of the year-to-year changes was generally in agreement between tower and modeled data (Fig. 8).

Tower and model data generally showed that monthly R_e anomalies were correlated with monthly GPP anomalies (Table 4). Soil drought would tend to affect GPP and R_e similarly, which would explain that general correlation. Cool temperatures would likely reduce R_e but not

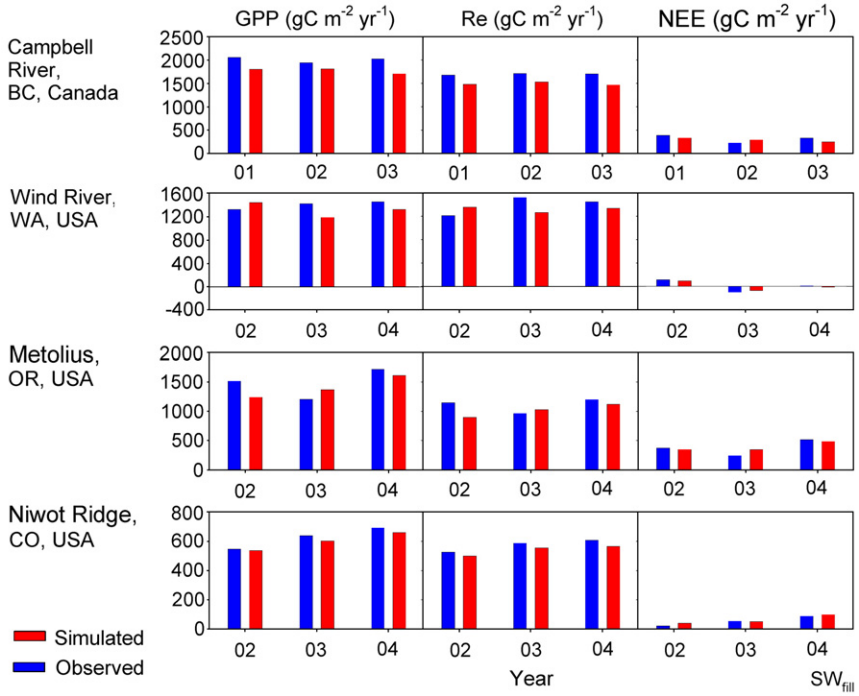

Fig. 8. Interannual variation in gross primary production (GPP), ecosystem respiration (R_e), and net ecosystem exchange (NEE) for tower observations and model simulations. The SW_{fill} FPAR and site level optimizations were used.

Table 4
Relationships of monthly anomalies (anom) for gross primary production (GPP), ecosystem respiration (R_e), and net ecosystem exchange (NEE).

Site	Tower		Model	
	Best fit	R^2	Best fit	R^2
NEP anom vs. GPP anom				
CR	$y=-0.11x-0.01$	0.01	$y=43x+0.01$	0.26
WR	$y=0.30x+0.00$	0.05	$y=0.62x+0.00$	0.82
ME	$y=0.59x+0.01$	0.82	$y=0.51x-0.01$	0.77
NR	$y=0.59x+0.01$	0.63	$y=0.54x-0.01$	0.66
NEP anom vs. R_e anom				
CR	$y=-0.57x-0.01$	0.62	$y=-0.34x+0.00$	0.13
WR	$y=-0.70x+0.00$	0.59	$y=0.65x-0.00$	0.21
ME	$y=0.70x+0.01$	0.28	$y=0.55x+0.01$	0.28
NR	$y=0.09x+0.00$	0.00	$y=0.26x-0.01$	0.05
GPP anom vs. R_e anom				
CR	$y=0.43x-0.00$	0.48	$y=0.66x-0.00$	0.38
WR	$y=0.30x-0.01$	0.21	$y=1.66x-0.01$	0.63
ME	$y=1.70x-0.00$	0.70	$y=1.55x-0.01$	0.76
NR	$y=1.01x-0.01$	0.44	$y=1.26x-0.01$	0.58

FPAR type is SW_{fill} and optimization type is site-specific.

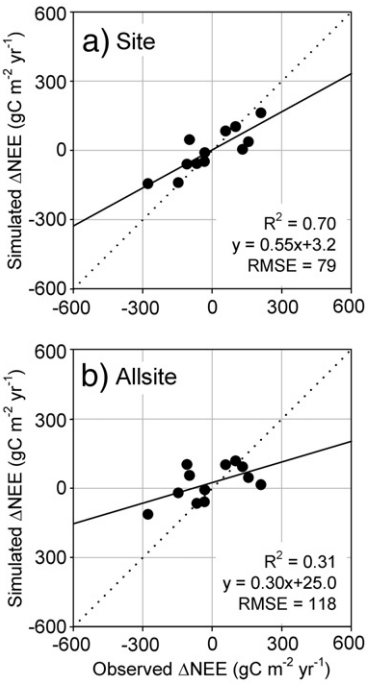

Fig. 9. Relationship of the sign and magnitude of year-to-year change in NEE using a) site-level parameter optimizations and b) a cross-site optimization. Each point represents one year-to-year change at one site.

necessarily GPP, which would tend to weaken the correlation of the GPP and R_e anomalies. NEE monthly anomalies were strongly correlated with GPP anomalies at the ME and NR sites in both tower and model data. In contrast, the NEE anomalies were most correlated with the R_e anomalies at WR and CR in the tower data. There was only weak correlation of NEE anomalies with R_e anomalies in the model data.

3.3. Cross-site and off-site parameter optimization

In the cross-site optimizations, the parameter values selected were generally intermediate among the ranges of values selected in the site-specific optimizations (Table 3). The accuracy of the site-level simulations was correspondingly reduced in the case of the cross-site optimization. Using the parameters optimized across sites, RMSE always increased for GPP through not always for NEE (Table 5) compared with using parameters optimized at the site level. The ability to capture interannual variation in NEE was also reduced (Fig. 9).

When parameters from one site were used at other sites, the RMSEs increased. Using WR parameters at the other sites caused the mid growing season residuals for GPP and R_e to generally increase relative to the site-level parameterization (Fig. 10). In the case of GPP, the more positive residuals (model underestimates) were primarily because of the greater sensitivity to VPD at WR (Table 3) and relatively high VPDs elsewhere, especially at MR. In the case of R_h, the higher residuals were primarily because of the relatively low sensitivity of R_h to temperature at WR (Table 3) which tended to cause underestimates elsewhere.

The cross-site, cross-year RMSEs for GPP were similar in each case where the site-specific parameter values were used across all sites. The RMSEs for R_e varied more widely (1.33–2.36) (Fig. 11).

Table 5
Root Mean Square Error (RMSE) at the site level for gross primary production (GPP), ecosystem respiration (R_e) and net ecosystem exchange (NEE) using site-specific and cross-site parameter optimization.

	Site			
	CR	WR	ME	NR
GPP				
$RMSE_{site}$	1.48	1.69	1.21	0.68
$RMSE_{cross\text{-}site}$	1.90	2.15	1.50	0.77
R_e				
$RMSE_{site}$	1.30	1.69	1.21	0.68
$RMSE_{cross\text{-}site}$	2.13	1.58	1.07	0.50
NEE				
$RMSE_{site}$	1.18	1.40	1.00	0.52
$RMSE_{cross\text{-}site}$	1.19	1.46	0.99	0.72

4. Discussion

4.1. FPAR issues

Both the MODIS and SeaWiFS FPAR products are based on surface reflectance data and radiative transfer modeling (Myneni et al., 2002; Gobron et al., 2006). Despite an 8–10 day compositing period, many bin periods remained at these sites that were continuously overcast at the overpass time (12:00 for MODIS and 13:30 for SeaWiFS, local time). Once the intervals with low quality data were filled with the Zhao et al. algorithm (2005), a mostly stable FPAR trajectory was produced. The $MODIS_{TS}$ smoothing clearly reduces some artifactual short term variation in the $MODIS_{fill}$ product. The week-to-week variation remaining after filling/smoothing is especially low in the summer growing season when FPAR is most important in diagnostic models.

The absolute magnitude of the FPAR estimates was consistently high for the MODIS products, with summertime FPARs on the order of 0.95 across all sites. These high FPARs are accurate at the two high LAI sites (CR and WR) but are clearly overestimates at MR and NR where LAIs are much lower. A tendency for the MODIS product to overestimate FPAR has also been observed in other biomes (Fenshlot et al., 2004; Turner et al., 2005), with apparently some improvements on this issue between Collections 3 and 4. The Enhanced Vegetation Index (EVI) is also produced from the MODIS reflectances and was designed to address the saturation issue (Huete et al., 2002). EVI is theoretically an indicator of chlorophyll FPAR and is used as a substitute for FPAR in several diagnostic carbon flux models (Xiao et al., 2004; Sims et al., 2008), but the saturation issue has not been examined.

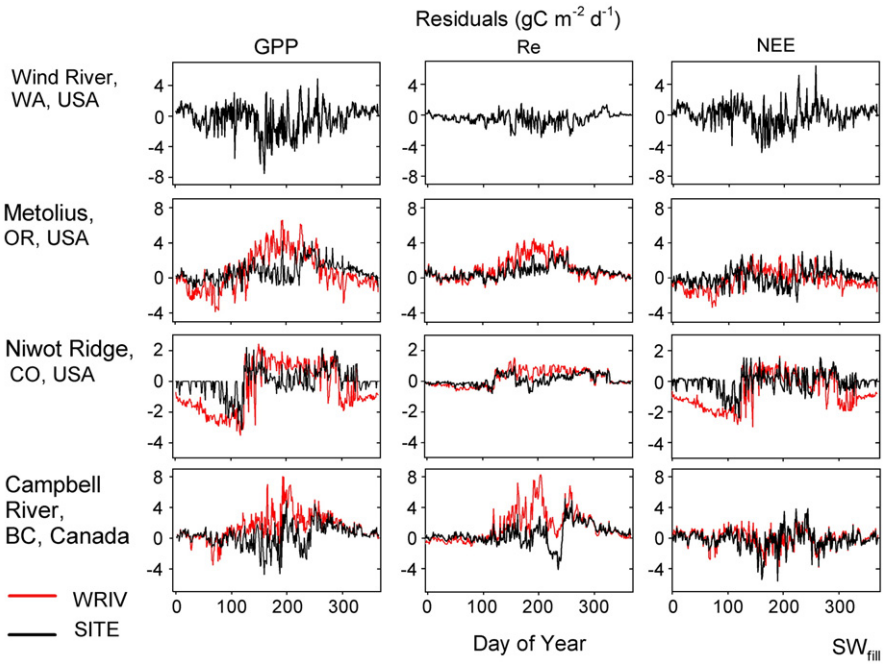

Fig. 10. Time series of the residuals for gross primary production (GPP), ecosystem respiration (R_e), and net ecosystem exchange (NEE). The year is 2002. Each panel has the residual (model − tower) for its site optimization and the residual when run with the parameters from the Wind River site optimization.

The SeaWiFS FPARs had maximum values of about 0.6 at CR and WR, which were clearly underestimates. Maximum values at MR and NR were about 0.3 which were also consistent underestimates. One factor here may be that the 3 cell by 3 cell averages covered a large enough area (~6.6×6.6 km) that it included areas with lower FPAR than the tower site. Nevertheless, because of the greater dynamic range between low and high FPAR sites there appears to be more information on broad geographical patterns in FPAR in the SeaWiFS product at these conifer forest sites compared to the MODIS product.

At the NR site, there are periods of snow cover every year and these seem to be registered on the MODIS product but not the SW product. In contrast, snow is rare at the CR site but both FPAR products there show seasonality in FPAR, probably related to issues with cloudiness. In any case, the apparent FPAR artifacts during the winter at these sites have little effect on simulated fluxes because incident PAR and Tmin are relatively low already.

For the most part, FPAR does not vary much interannually at conifer sites, which is consistent with the similar satellite-based estimates for midsummer FPARs across years at these sites. Large changes in MODIS and SeaWiFS FPAR products have been observed at conifer sites after large disturbances such as fire (Turner et al., 2006; Gobron et al., 2006).

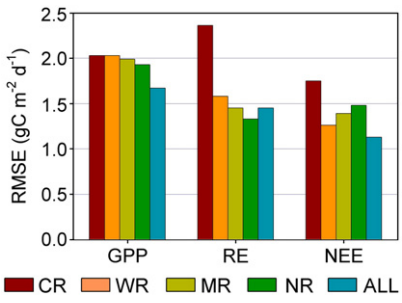

Fig. 11. Effect on cross-site Root Mean Square Error (RMSE) of using site-specific parameters when running across sites. CR = Campbell River, WR = Wind River, MR = Metolius River, NR = Niwot Ridge, All = cross-site.

The more accurate simulations of NEE using SW_{fill} for the cross-site optimization compared to using the MODIS products (Table 2, Fig. 3) would be expected because the lower FPARs in SW_{fill} at the less productive sites is providing the simulation with more information than is the case with $MODIS_{fill}$. The difference between outputs based on $MODIS_{fill}$ and SW_{fill} is greatest at the low LAI sites like NR (Fig. 4). The artifactually high FPAR in $MODIS_{fill}$ tends to push the GPP and R_e too high there. The optimized base rates for R_m and R_h were high in the case of the SW_{fill} optimization (Table 2) because both R_m and R_h are driven by FPAR and since the FPARs are low, the optimized base rates are high.

The RMSEs for the $MODIS_{TS}$ FPAR were less than or equal to those for the $MODIS_{fill}$ FPAR. The modest benefits are a function of smoothing out artifactual short term variation associated with clouds. Nightengale et al. (2009) showed a similar modest effect of the TIMESAT smoothing when the product was used in CASA, another diagnostic carbon flux model.

4.2. Variation in site-level parameterization

The sites differed widely in the maximum and average values for GPP. The maximum values for tower GPP were greatest at CR, intermediate at WR and MR, and lowest at NR. These values are consistent with expectations based on climate and stand age: NR is the coldest site and the low maximum GPP is associated with a conservative ecophysiological strategy often found in trees in extreme environments (Woodward, 1995). The stand age at NR is also relatively high, which probably introduces an additional constraint on productivity (Gower et al., 1996). CR has a mild climate and is a relatively young stand, thus has higher maximum GPP. The WR site is unusual in having relatively old trees (~450 yrs), which may account for the lower maximum GPP. The MR site is young for Ponderosa pine but often experiences effects of high VPDs and soil drought on GPP.

With site-level optimization, the CFLUX simulations of GPP generally agreed well with the tower data. One exception was a period of high GPP in the simulations at NR in 2004 driven by an artifactual bump in the FPAR (Figs. 2 and 5). A second exception was the days of artificially low GPP in mid summer at WR. The optimization there

selected VPD limits of 0 and 2500 Pa, which were low relative to the limits selected at the other sites and tended to make the simulations over sensitive to VPD.

As would be expected because of its low productivity, the observed clear-sky LUE (Table 1) and optimized maximum LUE (Table 3) were lowest at NR among the sites. Values for maximum LUE ranged from 3 to 4 gC MJ^{-1} at the other sites, close to the maximum physiologically possible LUE. Note that these values would be achieved only under overcast skies, low VPD, and moderate temperatures.

The optimized values for minimum temperature parameters were similar across sites and were similar to the values used in the MOD17 diagnostic model in global runs with MODIS data (Running et al., 2000). The optimization did not use the Tmin scalar at WR, possibly because incident PAR was a better predictor. The optimization selected a relatively low VPD minimum and maximum at WR and this may reflect a conservative ecophysiology associated with the quite old trees there.

The maximum R_e in the observations generally followed the pattern in maximum GPP, with CR>WR>MR>NR. After optimizing the base rates for R_m and R_h, the simulations showed generally good agreement with the observations. The optimized values for the base rate of R_m were conspicuously low at CR (Table 3) which is consistent with it being a relatively young stand in a favorable site. The optimized base rate for R_h was also relatively low at CR but the temperature sensitivity for R_h was much higher than at the other sites, thus apparently compensating for the lower base rate.

The observations showed strong site-specific differences in the relative importance of GPP vs. R_e monthly anomalies in explaining NEE monthly anomalies. At MR and NR, the NEE anomaly was more closely correlated with the GPP anomaly whereas at CR and WR it was the R_e anomaly. This difference could be interpreted as a greater sensitivity of the R_m component of R_e at CR and WR because LAI and aboveground biomass were much greater (Falk et al., 2008). The modeled NEE anomalies were most strongly driven by GPP anomalies in all cases. The difference at the high LAI sites may be due to an underestimation of R_m because the values of SeaWiFS FPARs are artifactually low. Nevertheless, the model did account for 70% of the year to year variation in NEE across all sites (Fig. 9).

4.3. Cross-site parameter optimization

The increase in error when running with parameters optimized across all sites is expected because parameters optimized at the site level differed from those derived from the cross-site optimization in some cases. The RMSE increase was less than 25% except in one case (NEE at NR). There were much larger increases in error in some cases when parameters optimized at one site were used across all sites (Fig. 11). The cross-site RMSE for NEE was between 1.26 and 1.75 with the site-specific optimization and was 1.13 with the cross-site optimization. This response indicates the benefits of a multiple site parameter optimization approach.

With the increase in number of flux towers either currently or previously supported in each biome, the possibilities for alternative parameter optimization schemes is growing. The ecoregion (Omernik, 1987) is a natural level at which to stratify available towers and two or more tower sites can be found in most of the Level I ecoregions in North America (CEC, 2008). Further research is needed on the possible trade-offs of using a single tower site in a Level II or Level III ecoregion (higher levels are more narrowly defined) vs. multiple towers sites in a Level I ecoregion. In Turner et al. (2006), CFLUX was optimized by vegetation cover type for the Level 3 ecoregions in western Oregon but that required using outputs from the Biome-BGC model run at selected points as reference data because there were insufficient towers. Either multiple sites within Level I ecoregions or single sites within higher level ecoregion stratifications would be an improvement over a single site per ecoregion at a low level of ecoregion stratification.

5. Conclusions

Diagnostic carbon cycle models are increasingly used to monitor terrestrial gross ecosystem exchange, ecosystem respiration, and net ecosystem exchange at regional to global scales. FPAR products from different sensors vary widely in their absolute values for particular sites and their dynamic range across sites. Site-specific parameter optimization at eddy covariance flux tower sites can produce simulations with good fits to observational data but optimized parameters may vary across sites within a biome. For large area simulations, a cross-site parameter optimization within a given vegetation cover type will reduce prediction error compared with a single site optimization.

Acknowledgements

We thank Nadine Gobron (Joint Research Center) for the SeaWiFS FPAR data and Joanne Nightengale (NASA Goddard Space Flight Center) for the help in interpretation of the $MODIS_{TS}$ data. This research was supported by the U.S. Department of Energy Biological and Environmental Research Terrestrial Carbon Program (Award # DE-FG02-04ER63917).

References

Adair, E. C., Parton, W. J., Del Grosso, S. J., Silver, W. L., Harmon, M. E., Hall, S. A., et al. (2008). Simple three-pool model accurately describes patterns of long-term decomposition in diverse climates. *Global Change Biology*, *14*, 2636—2660.

Baldocchi, D., Falge, E., Gu, L., Olson, R., Hollinger, D., Running, S., et al. (2001). FLUXNET: A new tool to study the temporal and spatial variability of ecosystem-scale carbon dioxide, water vapor, and energy flux densities. *Bulletin of the American Meteorological Society*, *82*, 2415—2434.

Canadell, J. G., Le Quere, C., Raupach, M. R., Field, C. B., Buitenhuis, E. T., Ciais, P., et al. (2007). Contributions to accelerating atmospheric CO_2 growth from economic activity, carbon intensity, and efficiency of natural sinks. *Proceedings of the National Academy of Sciences of the United States of America*, *104*, 18866—18870.

CEC (2008). Center for environmental cooperation. *Level I Ecoregions of North America* http://www.cec.org/home/index.cfm?varlan=english

Cohen, W. B., Maiersperger, T. K., Turner, D. P., Ritts, W. D., Pflugmacher, D., Kennedy, R. E., et al. (2006). MODIS land cover and LAI Collection 4 product quality across nine sites in the western hemisphere. *IEEE Transactions on Geosciences and Remote Sensing*, *44*, 1843—1857.

Densai, A. R., Richardson, A. D., Moffat, A. M., Kattge, J., Hollinger, D. Y., Barr, A., et al. (2008). Cross-site evaluation of eddy covariance GPP and RE decomposition techniques. *Agricultural and Forest Meteorology*, *148*, 821—838.

Drolet, G. G., Middleton, E. M., Huemmrich, K. F., Hall, F. G., Amiro, B. D., Barr, A. G., et al. (2008). Regional mapping of gross light-use efficiency using MODIS spectral indices. *Remote Sensing of Environment*, *112*, 3064—3078.

Falge, E., Baldocchi, D., Tenhunen, J., Aubinet, M., Bakwin, P., Berbigier, P., et al. (2002). Seasonality of ecosystem respiration and gross primary production as derived from FLUXNET measurements. *Agricultural and Forest Meteorology*, *113*, 53—74.

Falk, M., Wharton, S., Schroeder, M., Ustin, S. L., & Paw, K. T. (2008). Flux partitioning in an old-growth forest: Seasonal and interannual dynamics. *Tree Physiology*, *28*, 509—520.

Fenshlot, R., Sandholt, I., & Rasmussen, M. S. (2004). Evaluation of MODIS LAI, fAPAR and the relation between fAPAR and NDVI in a semi-arid environment using in situ measurements. *Remote Sensing of Environment*, *91*, 490—507.

Fensholt, R., Sandholt, I., & Stisen, S. (2006). Evaluating MODIS, MERIS, and VEGETATION — Vegetation indices using in situ measurements in a semiarid environment. *IEEE Transactions on Geoscience and Remote Sensing*, *44*, 1774—1786.

Fu, P., & Rich, P. M. (1999). *Proceedings of the 19th Annual ESRI User Conference, San Diego, USA*.

Goa, F., Morisette, J., Wolfe, R., Ederer, G., Pedelty, J., Masuoka, E., et al. (2008). An algorithm to produce temporally and spatially continuous remote sensing time series data: An example using MODIS LAI. *IEEE Geoscience and Remote Sensing Letters*, *5*, 60—64.

Gobron, N., Pinty, B., Aussedat, O., Chen, J. M., Cohen, W. B., Fensholt, R., et al. (2006). Evaluation of fraction of absorbed photosynthetically active radiation products for different canopy radiation transfer regimes: Methodology and results using Joint Research Center products derived from SeaWiFS against ground-based estimations. *Journal of Geophysical Research — Atmospheres*, *111*, D13110.

Gobron, N., Pinty, B., Aussedat, O., Taberner, M., Faber, O., Melin, F., et al. (2008). Uncertainty estimates for the FAPAR operational products derived from MERIS — Impact of top-of-atmosphere radiance uncertainties and validation with field data. *Remote Sensing of Environment*, *112*, 1871—1883.

Gower, S. T., McMurtrie, R. E., & Murty, D. (1996). Above ground net primary production decline with stand age: potential causes. *Trends in Ecology and Evolution*, *11*, 378—382.

Huete, A., Didan, K., Miura, T., Rodriguez, E. P., Gao, X., & Ferreira, L. G. (2002). Overview of the radiometric and biophysical performance of the MODIS vegetation indices. *Remote Sensing of Environment*, *83*, 195—213.

Humphreys, E. R., Black, T. A., Morgenstern, K., Cai, T. B., Drewitt, G. B., Nesic, Z., et al. (2006). Carbon dioxide fluxes in coastal Douglas-fir stands at different stages of development after clearcut harvesting. *Agricultural and Forest Meteorology*, *140*, 6—22.

Irvine, J., Law, B. E., Martin, J. G., & Vickers, D. (2008). Interannual variation in soil CO_2 efflux and the response of root respiration to climate and canopy gas exchange in mature ponderosa pine. *Global Change Biology*, *14*, 2848—2859.

Jarvis, P. G., & Leverenz, J. W. (1983). Ecosystem processes: Mineral cycling, productivity, and man's influence. In O. L. Lange, P. S. Nobel, P. S. Osmond, & H. Ziegler (Eds.), *Ecosystem Processes: Mineral Cycling, Productivity, and Man's Influence* (pp. 233—280). New York: Springer-Verlag.

Jonsson, P., & Eklundh, L. (2004). TIMESAT — A program for analyzing time-series of satellite sensor data. *Computers and Geosciences*, *30*, 833—845.

LaFont, S., Kergoat, L., Dedieu, G., Chevillard, A., Karstens, U., & Kolle, O. (2002). Spatial and temporal variability in land CO_2 fluxes estimated with remote sensing and analysis over western Eurasia. *Tellus Series B-Chemical and Physical Meteorology*, *54*, 820—833.

Law, B. E., Falge, E., Gu, L., Baldocchi, D., Bakwin, P., Berbigier, P., et al. (2002). Environmental controls over carbon dioxide and water vapor exchange of terrestrial vegetation. *Agricultural and Forest Meteorology*, *113*, 97—120.

LPDAAC (2008). *Land Process Distributed Active Archive Center.* https://lpdaac.usgs.gov/

Mahadevan, P., Wofsy, S. C., Matross, D. M., Xiao, X. M., Dunn, A. L., Lin, J. C., et al. (2008). A satellite-based biosphere parameterization for net ecosystem CO_2 exchange: Vegetation Photosynthesis and Respiration Model (VPRM). *Global Biogeochemical Cycles*, *22*, GB2005.

Makela, A., Pulkkinen, M., Kolari, P., Lagergren, F., Berbigier, P., Lindroth, A., et al. (2008). Developing an empirical model of stand GPP with the LUE approach: Analysis of eddy covariance data at five contrasting conifer sites in Europe. *Global Change Biology*, *14*, 92—108.

Medlyn, B. E., Robinson, A. P., Clement, R., & McMurtrie, R. E. (2005). On the validation of models of forest CO_2 exchange using eddy covariance data: Some perils and pitfalls. *Tree Physiology*, *25*, 839—857.

Myneni, R., Hoffman, R., Knyazikhin, Privette, Y. J., Glassy, J., & Tian, H. (2002). Global products of vegetation leaf area and fraction absorbed PAR from one year of MODIS data. *Remote Sensing of Environment*, *76*, 139—155.

NACP (2008). *MODIS for NACP.* http://accweb.nascom.nasa.gov/

Nightengale, J., Morisette, J., Wolfe, R., Tan, B., Gao, F., Ederer, G., et al. (2009). Temporally smoothed and gap-filled MODIS land products for carbon modeling: Application of the FPAR product. *International Journal of Remote Sensing*, *30*, 1083—1090.

Omernik, J. M. (1987). Ecoregions of the conterminous United States. Map (scale 1:7,500,000). *Annals of the Association of American Geographers*, *77*, 118—125.

Potter, C. S., Randerson, J. T., Field, C. B., Matson, P. A., Vitousek, P. M., Mooney, H. A., et al. (1993). Terrestrial ecosystem production, a process model based on global satellite and surface data. *Global Biogeochemical Cycles*, *7*, 811—841.

Running, S. W., Baldocchi, D. D., Turner, D. P., Gower, S. T., Bakwin, P. S., & Hibbard, K. A. (1999). A global terrestrial monitoring network integrating tower fluxes, flask sampling, ecosystem modeling and EOS satellite data. *Remote Sensing of Environment*, *70*, 108—128.

Running, S. W., Thornton, P. E., Nemani, R., & Glassy, J. M. (2000). Global terrestrial gross and net primary productivity from the Earth Observing System. In O. E. Sala, R. B. Jackson, H. A. Mooney, & R. W. Howarth (Eds.), *Methods in Ecosystem Science* (pp. 44—57). New York: Springer-Verlag.

Sacks, W. J., Schimel, D. S., & Monson, R. K. (2007). Coupling between carbon cycling and climate in a high-elevation subalpine forest: A model-data fusion analysis. *Oecologia*, *151*, 54—68.

Sims, D. A., Rahman, A. F., Cordova, V. D., El-Masri, B. Z., Baldocchi, D. D., Bolstad, P. V., et al. (2008). A new model of gross primary productivity for North American ecosystems based solely on the enhanced vegetation index and land surface temperature from MODIS. *Remote Sensing of Environment*, *112*, 1633—1646.

Stenberg, P. (1996). Correcting LAI-2000 estimates for the clumping of needles in shoots of conifers. *Agricultural and Forest Meteorology*, *79*, 1—8.

Thomas, C.K., Law, B.E., Irvine, J., Martin, J.G., Pettijohn, J.C., & Davis, K.J., (in review). Interannual and seasonal variation in carbon and water exchange at a semi-arid mature Ponderosa Pine site in Central Oregon. *Global Change Biology*.

Turner, D. P., Ollinger, S. V., & Kimball, J. S. (2004). Integrating remote sensing and ecosystem process models for landscape to regional scale analysis of the carbon cycle. *BioScience*, *54*, 573—584.

Turner, D. P., Ritts, W. D., Cohen, W. B., Maeirsperger, T., Gower, S. T., Kirschbaum, A., et al. (2005). Site-level evaluation of satellite-based global terrestrial gross primary production and net primary production monitoring. *Global Change Biology*, *11*, 666—684.

Turner, D. P., Ritts, W. D., Styles, J. M., Yang, Z., Cohen, W. B., Law, B. E., et al. (2006). A diagnostic carbon flux model to monitor the effects of disturbance and interannual variation in climate on regional NEP. *Tellus B*, *58*, 476—490.

Waring, R. H., Landberg, J. J., & Williams, M. (1998). Net primary production of forest: A constant fraction of gross primary production? *Tree Physiology*, *18*, 129—134.

Woodward, F. I. (1995). Ecophysiological controls of conifer distribution. In W. K. Smith, & T. M. Hinckley (Eds.), *Ecophysiology of Coniferous Forests* (pp. 79—94). San Diego CA: Academic Press.

Xiao, X., Zhang, Q., Braswell, B. H., Urbanski, S., Boles, S., Wofsy, S. C., et al. (2004). Modeling gross primary production of temperate deciduous broadleaf forest using satellite images and climate data. *Remote Sensing of Environment*, *91*, 256—270.

Zhao, M. S., Heinsch, F. A., Nemani, R. R., & Running, S. W. (2005). Improvements of the MODIS terrestrial gross and net primary production global data set. *Remote Sensing of Environment*, *95*, 164—176.